Magneto-Optical Functions at the 3*p* Resonances of Fe, Co, and Ni: *Ab initio* Description and Experiment

F. Willems,[1,*] S. Sharma,[1,†] C. v. Korff Schmising,[1] J. K. Dewhurst,[2] L. Salemi,[3] D. Schick,[1] P. Hessing,[1] C. Strüber,[1] W. D. Engel,[1] and S. Eisebitt[1,4]

[1]*Max Born Institute for Nonlinear Optics and Short Pulse Spectroscopy, Max-Born-Strasse 2A, 12489 Berlin, Germany*
[2]*Max-Planck-Institute for Microstructure Physics, Weinberg 2, 06120 Halle (Saale), Germany*
[3]*Department of Physics and Astronomy, Materials Theory, Uppsala University, 75120 Uppsala, Sweden*
[4]*Institut für Optik und Atomare Physik, Technische Universität Berlin, 10623 Berlin, Germany*

(Received 20 December 2018; published 31 May 2019)

We present experimental data and a complete theoretical description of the magneto-optical contributions to the complex refractive index in the extreme ultraviolet (XUV) range covering the 3*p* resonances of Fe, Co, and Ni. The direct comparison of the two allows us to conclude that many-body corrections to the ground state and local field effects are crucial for an accurate description of *M*-edge spectra. Our results are relevant for investigation of static magnetization, via XUV spectroscopy of multielement systems, as well as the dynamics of magnetization, as needed in the study of femtomagnetism and spintronics.

DOI: 10.1103/PhysRevLett.122.217202

X-ray spectroscopy is a very powerful tool as it can probe the electronic and magnetic structure for each constituent element of a material separately via transitions from core levels to unoccupied states [1]. Magnetic order is probed via dichroism, which is a contrast based on the projection vector of the x-ray polarization onto the sample magnetization. The element selectivity stems from the increased scattering cross section when the incident x-ray photon energy is tuned to resonate with transitions from core levels, which are energetically separated for different atoms and in different chemical environments. For the important class of magnetically ordered materials containing 3*d* transition metals (TMs), the use of *L*-edge (2*p* core levels) spectroscopy at synchrotron facilities was dominant to determine magnetic properties, due to the large magnitude of the magnetic dichroism at these transitions and the ability to apply sum rules to disentangle spin and orbital contributions to the magnetic moments [1,2]. In recent years, however, the use of magnetic dichroism in the extreme ultraviolet regime, exploiting the *M*-edge resonances (3*p* core levels) in 3*d* TMs, has strongly increased due to the growing availability of laboratory-based high harmonic generation (HHG) sources [3–8].

The major drawback of these *M*-edge experiments is the challenging data interpretation due to the following: (a) The strong overlap of the spin-orbit split core levels ($3p_{3/2,1/2}$) implies that the optical sum rules cannot be applied to disentangle spin and orbital contributions in the total angular moment. (b) The *M*-edge resonances of the 3*d* TMs exhibit substantial overlap with each other for photon energies above and, in particular, well below the absorption edges [4,6,9–11]. This has led to several unresolved controversies in the interpretation of the experimental data to reconcile which one requires a fully parameter-free theoretical description to base the interpretation of the experimental data on. However, all previous calculations of *M*-edge spectra even for the most common 3*d* TMs (Fe, Co, and Ni) rely on *ad hoc* Gaussian broadening, energy shifts, and amplitude scaling [12–14] to bring theoretical results close to experiments.

In the present Letter, we combine experimental and theoretical studies for the 3*d* TMs Fe, Co, and Ni at their *M*-edge resonances. Experimentally, we measured both the dispersive and absorptive parts of the magneto-optical (MO) contributions to the refractive index, eliminating the need to complement information by a Kramers-Kronig analysis [15], which is inherently inaccurate when applied to rapidly changing functions measured in a small energy window. Theoretically, we provide a fully *ab initio* description of these spectra. The important breakthrough of this Letter is that we find the *ab initio* calculations to be in unprecedentedly good agreement with the accurate experimental results. With this we are also able to provide the fundamental reasons behind previous discrepancies between theory and experiment. Most importantly, we are able to assign physical processes that lead to each feature in the experimental spectra, a prerequisite to disentangle signals from overlapping XUV-MO-based spectra in multicomponent materials. This will have direct and significant consequences not just for static but also dynamic spectral studies, crucial in the fields of femtomagnetism and spintronics.

The experiments were carried out at the BESSY II synchrotron facility on the beam line UE112-PGM-1. We performed independent XUV-magnetic circular dichroism (MCD) as well as Faraday rotation measurements, from which we retrieved the absorptive and the dispersive parts

of the MO functions, respectively. Magnetron sputtering was used to grow 15 nm thick layers of Fe, Co, and Ni on Si_3N_4 membranes of 20 nm thickness, capped by a 3 nm Al layer oxidation protection. All of the films have their magnetic easy axis in the sample plane and exhibit a coercivity of < 10 mT.

In the XUV-MCD measurement we recorded the transmitted intensity ($I_\pm$) of circularly polarized light through the sample for two magnetic field directions $(+,-)$ as a function of photon energy ($\hbar\omega$). We calculate the XUV-MCD as $D = 0.25\log(I_+/I_-)$. In the Faraday rotation measurement, linearly polarized XUV light is transmitted through the sample for two magnetization directions $(+,-)$ and analyzed by an XUV polarimeter. The Faraday rotation angle Φ_F as function of incident photon energy is retrieved via the magnetic asymmetry $A = (I_{R+} - I_{R-})/(I_{R+} + I_{R-})$ as $\Phi_F = 1/2\arcsin(A/P)$, where P is the polarizing power of the polarimeter. In both measurements, the glancing angle of incidence on the sample was 50° and the sample magnetization was set via an in-plane electromagnet. By correcting for the angle of incidence and non-negligible refraction of the XUV light at the vacuum-sample interface, we retrieve the elemental MO functions independent of the experimental geometry.

Following Valencia *et al.* [15], we write the complex refractive index n for the two circularly polarized eigenmodes $(+,-)$ as

$$n_\pm(\omega) = 1 - [\delta(\omega) \pm \Delta\delta(\omega)] + i[\beta(\omega) \pm \Delta\beta(\omega)]. \quad (1)$$

The relation between the MO functions $(\Delta\delta(\omega), \Delta\beta(\omega))$ and the measured quantities D and Φ_F is in accordance with the work of Kuneš *et al.* [16] and written in Eq. (2). For simplicity, we stick here to the more compact relation (valid if refraction is neglected)

$$\Delta\delta(\omega) - i\Delta\beta(\omega) = \frac{c}{\omega d_t}\{-\Phi_F(\omega) + i[D(\omega)]\}, \quad (2)$$

where c is the speed of light in vacuum and d_t is the total thickness of the sample at a given angle of incidence. See the Supplemental Material for details [17], which includes Refs. [15,18–23]. We note that the term "MO functions" is used to describe what is traditionally called magneto-optical constants in order to emphasize the frequency dependence of these complex functions, which are analytic in the upper-half frequency plane.

Theoretically, the MO functions are calculated by first performing a ground-state calculation using density functional theory (DFT) within the local spin density approximation for the exchange-correlation potential [24]. A single shot GW calculation [25] is then employed to determine the position and width of the deep-lying (low in energy) $3p$ states. The Kohn-Sham $3p$ bands are then scissor shifted and broadened to mimic the GW spectral function. Subsequently, the response function is calculated using these Kohn-Sham states and the time-dependent extension of DFT, the so-called time-dependent density functional theory (TD-DFT) [26]. The linear response equation of TD-DFT reads as [27]

$$\varepsilon^{-1}(\omega) = 1 + \chi_0(\omega)\{1 - [v + f_{\mathrm{xc}}(\omega)]\chi_0(\omega)\}^{-1}, \quad (3)$$

where ε is the dielectric tensor, v is the Coulomb potential, χ_0 is the noninteracting response function, f_{xc} is the exchange-correlation kernel. Electron-hole correlations, which describe the excitonic effects, can be treated by the correct choice of this kernel [28]. The dielectric tensor is calculated by treating all quantities in Eq. (3) as complex valued matrices and hence avoiding the need for a Kramers-Kronig inversion. This dielectric tensor is related to the experimental MO functions by [18]

$$\Delta\delta(\omega) - i\Delta\beta(\omega) = 0.5i\varepsilon_{xy}(\omega)[\varepsilon_{xx}(\omega)]^{-1/2}. \quad (4)$$

All calculations are performed using the state-of-the-art full-potential linearized augmented plane wave [29] method as implemented in the ELK code [30,31].

In Fig. 1, we present both the experimentally determined real and imaginary parts of the MO functions and the *ab initio* calculated values for Fe, Co, and Ni. To the best of our knowledge, this is the first measurement of *both* the real and imaginary part of the MO functions at the $3p$ resonances for Fe, Co, and Ni, eliminating the errors associated with Kramers-Kronig analysis.

From the experimental data on the dichroic, absorptive part $\Delta\beta$ [Figs. 1(a)–1(c)], we make two observations. (1) All three elements show a significant off-resonant signal (≈10% of the maximum) extending from the lowest photon energy measured, i.e., 45 eV, up to the respective absorption edge. In the case of Ni, the off-resonant signal is detected up to 20 eV below the absorption edge. In Fe, we additionally observe a sizeable off-resonant signal above the absorption edge, extending up to 65 eV. (2) The maximum absolute amplitude of $\Delta\beta$ is smaller in Fe than in Co. This contradicts results at the L-edges [2] and earlier M-edge spectra [15] obtained via a Kramers-Kronig inversion. Experimentally, we find that the XUV-MCD amplitude does *not* necessarily scale with the atomic magnetic moment.

The measurement of the dispersive part of the MO functions $\Delta\delta$ [Figs. 1(d)–1(f)] reveals a very symmetric bipolar curve in Fe, while in Co and Ni the amplitude below the resonance energy is about 2 times the one above. We find the maximum positive amplitude in Co. The region where $\Delta\delta$ deviates from zero extends to at most 12 eV around the zero crossing of $\Delta\delta$ at resonance. Together with the off-resonant signal in the absorptive part, this finding is of great significance when investigating multilayer samples and alloys containing these elements, as their MO signals are spectrally overlapping. Thus, the exact knowledge of the MO functions allows us to predict the spectral shape and signal strength and hence elemental contributions

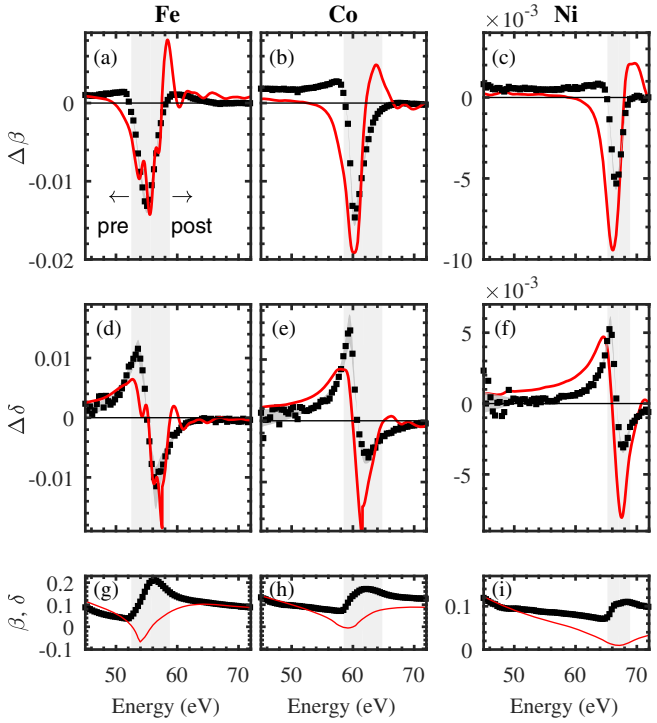

FIG. 1. Measured (black squares) and calculated (solid red line) MO functions. The area behind the data points is the error band. The regions for resonant $3p$-$3d$ transitions (determined by the x-ray absorption spectrum) are shaded in gray. The absorptive part ($\Delta\beta$) is shown in (a)–(c) for Fe, Co, and Ni, respectively. The dispersive part ($\Delta\delta$) is shown in (d)–(f). (g)–(i) show the optical functions (β measured and d taken from [22]) that were used to correct for refraction. The theoretical data was calculated using *GW* corrected Kohn-Sham bands and by solving the TD-DFT linear response equation including local field and excitonic effects. Fe and Co share the same axis scaling.

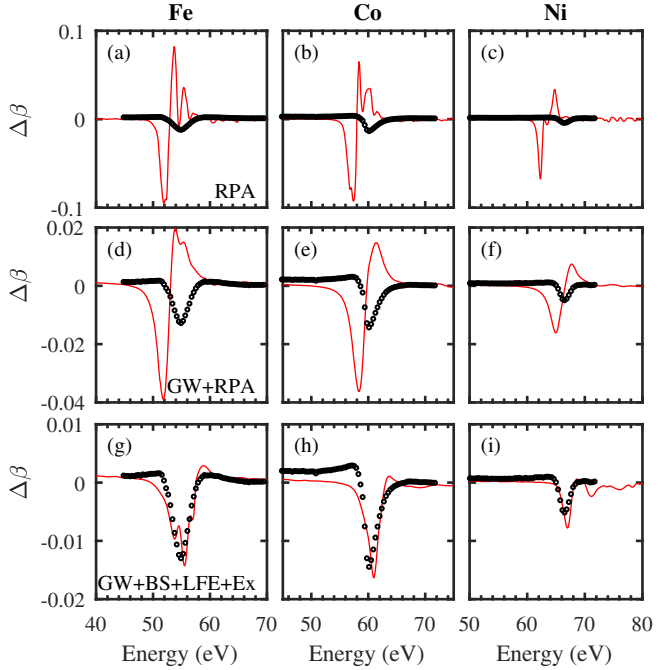

FIG. 2. Experimental (black dots) and theoretically calculated (red solid lines) $\Delta\beta$. Results obtained using Kohn-Sham bands and RPA, i.e., by using $f_{\mathrm{xc}} = 0$ in Eq. (3), are shown for (a) Fe, (b) Co, and (c) Ni. Results obtained using *GW* corrected Kohn-Sham bands to account for correct position and width of $3p$ states are presented for (d) Fe, (e) Co, and (f) Ni. Data obtained using *GW* corrected Kohn-Sham bands, by using $f_{\mathrm{xc}} = f_{\mathrm{xc}}^{\text{boot-strap}}$ to account for excitonic effects, by including local field effects by treating Eq. (3) as a matrix equation, and by *manually* reducing the $3p$ exchange splitting by 60%, are presented for (g) Fe, (h) Co, and (i) Ni.

expected in all XUV magneto-optical effects such as the magneto-optical Kerr effect in transverse, longitudinal, or polar geometry, as well as for XUV-MCD (e.g., [9,10, 32–34]). Moreover, in XUV scattering and imaging experiments, the choice of the photon energy not only determines the overall signal strength, but also the relative contribution of absorption vs phase contrast [35].

The parameter-free TD-DFT spectra in Fig. 1 are in good agreement regarding amplitude, spectral shape, and position of the resonance with the experimental data for all three elements. Note that both theory and experiments are plotted on the same absolute scales, without any adjustments. In order to analyze the reason behind past discrepancies and the significantly improved level of agreement between theory and experiment in the present Letter, and to explore the origin of various features in the XUV-MCD spectra, we probe our theoretical data in more detail. For this we discuss the three energy regions marked in Fig. 1 (pre-, at, and postresonance) separately.

At the resonance, experimental data show a well-defined peak (at 55.0, 60.3, and 66.6 eV for Fe, Co, and Ni, respectively). Calculations performed by using $f_{\mathrm{xc}} = 0$ in Eq. (3) [also known as the random phase approximation (RPA)] show significantly redshifted peaks with strongly overestimated amplitudes [see Figs. 2(a)–2(c)]. In the past it has been speculated [13] that underpinning this discrepancy could be missing many-body, core-hole, and excitonic effects in the Kohn-Sham band structure, which would (i) shift the $3p$ states to lower energies and (ii) broaden the $3p$ states. In order to investigate this, we have performed fully spin polarized *GW* calculations to determine the spectral function for bulk Fe, Co, and Ni. As expected, the many-body corrections have the effect of redshifting the $3p$ states as compared to the Kohn-Sham bands [see Figs. 3(d)–3(f)]. The many-body effects also lead to a finite width [36] of the $3p$ states. Their values are in close agreement with the experimental work of Nyholm *et al.* [37]. In contrast, the *GW* spectral function close to the Fermi level is almost the same as the Kohn-Sham density of states [see Figs. 3(a)–3(c)]. With this information in hand we can now correct the Kohn-Sham bands by redshifting and broadening the $3p$ states such that the Kohn-Sham density of states resemble the *GW* spectral function. This is

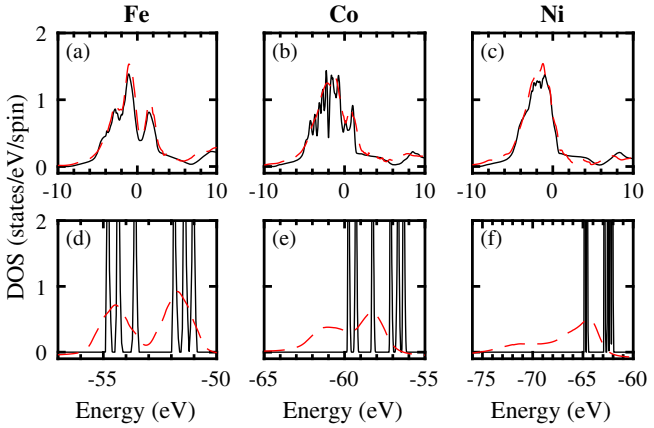

FIG. 3. Kohn-Sham (black lines) density of states and *GW* spectral function (red dashed lines) as a function of energy for the $3d$ (a)–(c) and the $3p$ (d)–(f) states of Fe, Co, and Ni. The calculations are fully spin-polarized; for demonstration purpose, here the spin-averaged quantities are shown.

a method for partially including many-body effects, while still keeping the whole procedure *ab initio*. The result of this is an energy shift of the resonant peak in the response functions by 0.1, 1.1, and 2.7 eV for Fe, Co, and Ni, respectively. While this brings the calculated resonance closer to the experiments [see Figs. 2(d)–2(f)], the discrepancy is still substantial for position, shape, and magnitude of the peak.

In order to find the missing piece in the calculation of the response function, we turn again to Eq. (3) and we note that χ_0 is a matrix in reciprocal space of vectors $\mathbf{G}$; this is due to the fact that an external perturbation of the type $e^{i(\mathbf{G}+\mathbf{q})\cdot\mathbf{r}}$ generates a response in the density of the form $e^{i(\mathbf{G}'+\mathbf{q})\cdot\mathbf{r}}$. Inversion of the matrix in $\mathbf{G}$ space allows for inclusion of the microscopic components known as the local field effects (LFEs) [27,28,38–41]. The latter can be understood in terms of a charge density rearrangement caused by the external perturbation (electric field of the incident electromagnetic XUV radiation), which in turn leads to creation of local microscopic fields. In addition to responding to the external perturbation, the system also responds to these local fields.

Local field effects have been ignored in all the past calculations [12–14] for Fe, Co, and Ni, as well as in the theoretical data shown in Figs. 2(a)–2(f). This approximation is in addition to the setting of the exchange-correlation kernel f_{xc} to zero in Eq. (3), which entails the neglect of electron-hole correlation (i.e., excitonic effects) in the response function.

In the following, we do include LFEs by solving Eq. (3) as a full matrix equation (we needed a matrix of 70×70 for convergence) and include excitonic effects by using the so-called boot-strap approximation for the kernel [28,40,41]. The results obtained using this advanced and parameter-free treatment (i.e., *GW* corrected Kohn-Sham bands + LFEs + excitons) are shown in Fig. 1 together with the experimental data for Fe, Co, and Ni, respectively. It is clear from these results that the TD-DFT spectra are now in excellent agreement with experiments in terms of both the position of the peak as well as its amplitude. We also note that, consistent with the experimental results, the maximum of the $\Delta\beta$ magnitude is smaller in Fe than in Co. This trend is entirely due to inclusion of the LFEs, which are strongest for Fe and weakest for Ni (i.e., inclusion of LFEs has much more effect on $\Delta\beta$ in Fe than in Ni). This was to be expected since the shallower $3p$ orbitals of Fe show a stronger overlap with $3d$ states as compared to the deeper-lying Ni $3p$ and valence $3d$ states. Therefore, according to the work of Aryasetiawan *et al.* [38] and Vast *et al.* [39], LFEs are expected to be larger in Fe. For L edges due to the small overlap of $2p$ and $3d$ states, LFEs are small.

The dramatic change in the quality of agreement between theory and experiments is almost entirely due to the inclusion of LFEs; calculations performed using $f_{\mathrm{xc}} = 0$ but including LFEs are almost indistinguishable from those using $f_{\mathrm{xc}}^{\text{boot-strap}}$. These results are a clear indication that, in calculations of the resonance peak in M-edge XUV-MCD spectra and similar observables, depending on the MO functions (a) the LFEs are crucial, (b) the *GW* corrections to the ground state are very important, and (c) excitonic effects do not play any role. The first two effects are highly material dependent and their relative importance cannot be established from the present work.

Turning to the postedge spectral region, one notes a large peak in the positive $\Delta\beta$ direction in the calculated data, which is absent in the experimental results. To investigate the origin of this peak, we focus on the exchange splitting of the $3p$ states, which is overestimated [42] by local spin density approximation [43–45]. To test how the exchange splitting effects the spectral response, we manually reduced the splitting by 60% [data shown in Figs. 2(g)–2(i)] and find an even better agreement with the experimental data. This is a clear indication that to treat postedge spectra one requires not only LFEs and *GW* corrections, but also improved ground-state spin density functionals to correctly describe the exchange splitting of semicore states. We hope that present results will stimulate future research in this direction.

As for the preedge part of the spectra, there are two questions that remain to be addressed: what leads to the finite weight of $\Delta\beta$ in the preedge energy region, in particular, for Co, and why do experiments show strikingly different behavior as compared to theory, namely, that there is a rise of $\Delta\beta$ just below the resonance. The answer to the first question we found to be the excitations from around the Fermi level to high-lying unoccupied states. Calculation without inclusion of high-lying states, more than 20 eV above the Fermi level, shows that the finite weight below the resonance vanishes. Despite our best attempts, we were unable to find the reason behind the peak just below the resonance.

To conclude, we provide accurate measurements and a reliable theoretical description of the magneto-optical functions for 3*d* transition metals in the XUV regime. Finding a good agreement between experiment and theory allows us to ascribe physical processes leading to the observed features. Many-body corrections to the ground state and local field effects are of crucial importance, while excitonic effects play no role. This puts 3*d* transition metal *M*-edge spectra—irrespective of their absorptive, dispersive, or mixed character in the specific spectroscopy employed—in the category where underlying physics can be entirely and accurately deciphered in a static and dynamic situation alike. Given the increased availability of femtosecond XUV laboratory sources, we expect this approach to be extremely useful in future studies of femtomagnetism and spintronics.

We thank P. Oppeneer for fruitful discussions. F. W. thanks R. Abrudan for support at the beam line. S. S., C. v. K. S., and S. E. would like to thank DFG for funding through TRR227 projects A02 and A04.

*willems@mbi-berlin.de
†sharma@mbi-berlin.de

[1] J. Stöhr and H. Siegmann, in *Magnetism*, edited by M. Cardona, P. Fulde, K. von Klitzing, R. Merlin, H.-J. Queisser, and H. Störmer (Springer, Berlin, 2006)

[2] F. Chen, C. T. Idzerda, Y. U. Lin, H.-J. Sette, C. T. Chen, Y. U. Idzerda, H.-J. Lin, N. V. Smith, G. Meigs, E. Chaban, G. H. Ho, E. Pellegrin, and F. Sette, Experimental Confirmation of the X-Ray Magnetic Circular Dichroism Sum Rules for Iron and Cobalt, Phys. Rev. Lett. **75**, 152 (1995).

[3] B. Vodungbo, A. Barszczak Sardinha, J. Gautier, G. Lambert, C. Valentin, M. Lozano, G. Iaquaniello, F. Delmotte, S. Sebban, J. Lüning, and P. Zeitoun, Polarization control of high order harmonics in the EUV photon energy range, Opt. Express **19**, 4346 (2011).

[4] O. Kfir, P. Grychtol, E. Turgut, R. Knut, D. Zusin, D. Popmintchev, T. Popmintchev, H. Nembach, J. M. Shaw, A. Fleischer, H. Kapteyn, M. Murnane, and O. Cohen, Generation of bright phase-matched circularly-polarized extreme ultraviolet high harmonics, Nat. Photonics **9**, 99 (2015).

[5] O. Kfir, E. Bordo, G. Ilan Haham, O. Lahav, A. Fleischer, and O. Cohen, In-line production of a bi-circular field for generation of helically polarized high-order harmonics, Appl. Phys. Lett. **108**, 211106 (2016).

[6] D. D. Hickstein, F. J. Dollar, P. Grychtol, J. L. Ellis, R. Knut, C. Hernández-García, D. Zusin, C. Gentry, J. M. Shaw, T. Fan, K. M. Dorney, A. Becker, A. Jaroń-Becker, H. C. Kapteyn, M. M. Murnane, and C. G. Durfee, Non-collinear generation of angularly isolated circularly polarized high harmonics, Nat. Photonics **9**, 743 (2015).

[7] C. von Korff Schmising, D. Weder, T. Noll, B. Pfau, M. Hennecke, C. Strüber, I. Radu, M. Schneider, S. Staeck, C. M. Günther, J. Lüning, A. E. D. Merhe, J. Buck, G. Hartmann, J. Viefhaus, R. Treusch, and S. Eisebitt, Generating circularly polarized radiation in the extreme ultraviolet spectral range at the free-electron laser FLASH, Rev. Sci. Instrum. **88**, 053903 (2017).

[8] J. L. Ellis, K. M. Dorney, D. D. Hickstein, N. J. Brooks, C. Gentry, C. Hernández-García, D. Zusin, J. M. Shaw, Q. L. Nguyen, C. A. Mancuso, G. S. Matthijs Jansen, S. Witte, H. C. Kapteyn, and M. M. Murnane, High harmonics with spatially varying ellipticity, Optica **5**, 479 (2018).

[9] S. Mathias, C. La-O-Vorakiat, P. Grychtol, P. Granitzka, E. Turgut, J. M. Shaw, M. Aeschlimann, M. M. Murnane, H. C. Kapteyn, R. Adam, H. T. Nembach, M. E. Siemens, S. Eich, C. M. Schneider, T. J. Silva, M. Aeschlimann, M. M. Murnane, and H. C. Kapteyn, Probing the timescale of the exchange interaction in a ferromagnetic alloy, Proc. Natl. Acad. Sci. U.S.A. **109**, 4792 (2012).

[10] E. Turgut, C. La-o-vorakiat, J. M. Shaw, P. Grychtol, H. T. Nembach, D. Rudolf, R. Adam, M. Aeschlimann, C. M. Schneider, T. J. Silva, M. M. Murnane, H. C. Kapteyn, and S. Mathias, Controlling the Competition between Optically Induced Ultrafast Spin-Flip Scattering and Spin Transport in Magnetic Multilayers, Phys. Rev. Lett. **110**, 197201 (2013).

[11] I. Radu, C. Stamm, A. Eschenlohr, F. Radu, R. Abrudan, K. Vahaplar, T. Kachel, N. Pontius, R. Mitzner, K. Holldack, A. Föhlisch, T. A. Ostler, J. H. Mentink, R. F. L. Evans, R. W. Chantrell, A. Tsukamoto, A. Itoh, A. Kirilyuk, A. V. Kimel, and T. Rasing, Ultrafast and distinct spin dynamics in magnetic alloys, SPIN **05**, 1550004 (2015).

[12] S. Valencia, A. Kleibert, A. Gaupp, J. Rusz, D. Legut, J. Bansmann, W. Gudat, and P. M. Oppeneer, Quadratic X-Ray Magneto-Optical Effect upon Reflection in a Near-Normal-Incidence Configuration at the *M* Edges of **3*d***3d-Transition Metals, Phys. Rev. Lett. **104**, 187401 (2010).

[13] E. Turgut, D. Zusin, D. Legut, K. Carva, R. Knut, J. M. Shaw, C. Chen, Z. Tao, H. T. Nembach, T. J. Silva, S. Mathias, M. Aeschlimann, P. M. Oppeneer, H. C. Kapteyn, M. M. Murnane, and P. Grychtol, Stoner versus Heisenberg: Ultrafast exchange reduction and magnon generation during laser-induced demagnetization, Phys. Rev. B **94**, 220408(R) (2016).

[14] D. Zusin, P. M. Tengdin, M. Gopalakrishnan, C. Gentry, A. Blonsky, M. Gerrity, D. Legut, J. M. Shaw, H. T. Nembach, T. J. Silva, P. M. Oppeneer, H. C. Kapteyn, and M. M. Murnane, Direct measurement of the static and transient magneto-optical permittivity of cobalt across the entire *M*-edge in reflection geometry by use of polarization scanning, Phys. Rev. B **97**, 024433 (2018).

[15] S. Valencia, A. Gaupp, W. Gudat, H.-C. C. Mertins, P. M. Oppeneer, D. Abramsohn, and C. M. Schneider, Faraday rotation spectra at shallow core levels: 3*p* edges of Fe, Co, and Ni, New J. Phys. **8**, 254 (2006).

[16] J. Kuneš, P. M. Oppeneer, H.-C. Mertins, F. Schäfers, A. Gaupp, W. Gudat, and P. Novák, X-ray Faraday effect at the $L_{2,3}$ edges of Fe, Co, and Ni: Theory and experiment, Phys. Rev. B **64**, 174417 (2001).

[17] See Supplemental Material at http://link.aps.org/supplemental/10.1103/PhysRevLett.122.217202 for experimental details, derivation of the equations, the impact of the refraction correction, error analysis, and the experimental data, which includes Refs. [15,18–23].

[18] P. M. Oppeneer, in *Handbook of Magnetic Material*, edited by K. Buschow (Elsevier, Amsterdam, 2001), Vol. 13, pp. 229–422.

[19] R. Abrudan, F. Brüssing, R. Salikhov, J. Meermann, I. Radu, H. Ryll, F. Radu, and H. Zabel, ALICE–An advanced reflectometer for static and dynamic experiments in magnetism at synchrotron radiation facilities, Rev. Sci. Instrum. **86**, 063902 (2015).

[20] J. Bahrdt, R. Follath, W. Frentrup, A. Gaupp, M. Scheer, R. Garrett, I. Gentle, K. Nugent, and S. Wilkins, Compensation of beam line polarizing effects at UE112 of BESSY II, AIP Conf. Proc. **1234**, 335 (2010).

[21] V. Lucarini, J. Saarinen, K.-E. Peiponen, and E. Vartiainen, *Kramers-Kronig Relations in Optical Materials Research*, Springer Series in Optical Sciences Vol. 110 (Springer-Verlag, Berlin, 2005).

[22] B. L. Henke, E. M. Gullikson, and J. C. Davis, X-ray interactions: Photoabsorption, scattering, transmission, and reflection at $E = 50 - 30000$ eV, $Z = 1 - 92$, At. Data Nucl. Data Tables **54**, 181 (1993).

[23] J. Stöhr and Y. Wu, in *New Directions in Research with Third-Generation Soft X-Ray Synchrotron Radiation Sources* (Springer Netherlands, Dordrecht, 1994), pp. 221–250.

[24] U. von Barth and L. Hedin, A local exchange-correlation potential for the spin polarized case. i, J. Phys. C **5**, 1629 (1972).

[25] L. Hedin, New Method for Calculating the One-Particle Green's Function with Application to the Electron-Gas Problem, Phys. Rev. **139**, A796 (1965).

[26] E. Runge and E. K. U. Gross, Density-Functional Theory for Time-Dependent Systems, Phys. Rev. Lett. **52**, 997 (1984).

[27] S. Sharma, J. K. Dewhurst, and E. K. U. Gross, in *First Principles Approaches to Spectroscopic Properties of Complex Materials*, edited by C. Di Valentin, S. Botti, and M. Cococcioni (Springer, Berlin, 2014), pp. 235–257.

[28] S. Sharma, J. K. Dewhurst, A. Sanna, and E. K. U. Gross, Bootstrap Approximation for the Exchange-Correlation Kernel of Time-Dependent Density-Functional Theory, Phys. Rev. Lett. **107**, 186401 (2011).

[29] D. J. Singh, *Planewaves Pseudopotentials and the LAPW Method* (Kluwer Academic Publishers, Boston, 1994).

[30] K. Dewhurst, S. Sharma, L. Nordström, F. Cricchio, O. Grånäs, and H. Gross, The ELK Code (2018), http://elk.sourceforge.net/.

[31] A $\mathbf{k}$-point grid of $20 \times 20 \times 20$ was used. All states greater than 95 eV below Fermi level were treated as Dirac spinors, i.e., obtained by solving the Dirac equation. All the other states are treated as Pauli spinors obtained by solving the Schrödinger equation, including spin-orbit and other relativistic corrections (e.g., mass correction and Darwin terms). All states up to 300 eV above the Fermi level were included in the calculations.

[32] C. La-O-Vorakiat, M. Siemens, M. M. Murnane, H. C. Kapteyn, S. Mathias, M. Aeschlimann, P. Grychtol, R. Adam, C. M. Schneider, J. M. Shaw, H. Nembach, and T. J. Silva, Ultrafast Demagnetization Dynamics at the *M* Edges of Magnetic Elements Observed Using a Tabletop High-Harmonic Soft X-Ray Source, Phys. Rev. Lett. **103**, 257402 (2009).

[33] D. Rudolf, C. La-O-Vorakiat, M. Battiato, R. Adam, J. M. Shaw, E. Turgut, P. Maldonado, S. Mathias, P. Grychtol, H. T. Nembach, T. J. Silva, M. Aeschlimann, H. C. Kapteyn, M. M. Murnane, C. M. Schneider, and P. M. Oppeneer, Ultrafast magnetization enhancement in metallic multilayers driven by superdiffusive spin current, Nat. Commun. **3**, 1037 (2012).

[34] F. Willems, C. T. L. Smeenk, N. Zhavoronkov, O. Kornilov, I. Radu, M. Schmidbauer, M. Hanke, C. von Korff Schmising, M. J. J. Vrakking, and S. Eisebitt, Probing ultrafast spin dynamics with high-harmonic magnetic circular dichroism spectroscopy, Phys. Rev. B **92**, 220405(R) (2015).

[35] A. Scherz, W. F. Schlotter, K. Chen, R. Rick, J. Stöhr, J. Lüning, I. McNulty, C. Günther, F. Radu, W. Eberhardt, O. Hellwig, and S. Eisebitt, Phase imaging of magnetic nanostructures using resonant soft x-ray holography, Phys. Rev. B **76**, 214410 (2007).

[36] Width for $3p_{1/2}$ and $3p_{3/2}$ states for Fe is 1.22, 0.76 eV, for Co is 1.25, 0.82 eV, and for Ni is 1.20, 1.20 eV, respectively.

[37] R. Nyholm, N. Martensson, A. Lebugle, and U. Axelsson, Auger and Coster-Kronig broadening effects in the 2p and 3p photoelectron spectra from the metals ^{22}Ti-^{30}Zn, J. Phys. F **11**, 1727 (1981).

[38] F. Aryasetiawan, O. Gunnarsson, M. Knupfer, and J. Fink, Local-field effects in NiO and Ni, Phys. Rev. B **50**, 7311 (1994).

[39] N. Vast, L. Reining, V. Olevano, P. Schattschneider, and B. Jouffrey, Local Field Effects in the Electron Energy Loss Spectra of Rutile TiO_2, Phys. Rev. Lett. **88**, 037601 (2002).

[40] S. Sharma, J. K. Drewhurst, A. Sanna, A. Rubio, and E. K. U. Gross, Enhanced excitonic effects in the energy loss spectra of LiF and Ar at large momentum transfer, New J. Phys. **14**, 053052 (2012).

[41] S. Sharma, J. K. Dewhurst, S. Shallcross, G. K. Madjarova, and E. K. U. Gross, Excitons in organics using time-dependent density functional theory: PPV, pentacene, and picene, J. Chem. Theory Comput. **11**, 1710 (2015).

[42] Calculated exchange splitting for $3p$ states is 2.7 eV for Fe, 2.2 eV for Co, and 0.9 eV for Ni.

[43] M. C. T. D. Müller, C. Friedrich, and S. Blügel, Acoustic magnons in the long-wavelength limit: Investigating the Goldstone violation in many-body perturbation theory, Phys. Rev. B **94**, 064433 (2016).

[44] K. Karlsson and F. Aryasetiawan, A many-body approach to spin-wave excitations in itinerant magnetic systems, J. Phys. Condens. Matter **12**, 7617 (2000).

[45] E. Şaşıoğlu, A. Schindlmayr, C. Friedrich, F. Freimuth, and S. Blügel, A many-body approach to spin-wave excitations in itinerant magnetic systems, Phys. Rev. B **81**, 054434 (2010).